Accuracy assessment of an integrated profiling technique for operationally deriving profiles of temperature, humidity, and cloud liquid water

Ulrich Löhnert,[1] Erik van Meijgaard,[2] Henk Klein Baltink,[2] Silke Groß,[1] and Reinout Boers[2]

[1]   An integrated profiling technique (IPT) for the simultaneous retrieval of the atmospheric state parameters temperature, humidity, and liquid water content profiles is assessed. The method combines measurements of a modern, ground-based profiling station equipped with a microwave profiler, cloud radar, and ceilometer, with the closest operational radiosonde measurement and standard surface-based meteorological measurements. All are combined within an optimal estimation procedure. The accuracy assessment is carried out in a virtual environment of a regional climate model. The model thermodynamic state is converted into the measurement space via so-called forward modeling. The IPT is then applied to the simulated measurements to retrieve the desired atmospheric state parameters which can be evaluated with the original model state. It is found that IPT-derived temperature and humidity profiles can add significant information for the time period between two operational radiosonde ascents, both if the measurements take place at the radiosonde site or if they are spatially apart. The benefits of a profiling station that applies an IPT can be valuable both for the reprocessing of dedicated field campaign data to obtain the best representation of the atmospheric state and for nowcasting and data assimilation applications. Depending on the density of the given operational radiosonde network, a ground-based profiling station has the potential of either significantly improving the quality of such a network or even substituting a small number of radiosonde stations. A further benefit of a ground-based profiling station is the retrieval of cloud microphysical properties, where IPT liquid water path retrieval accuracies show values better than 10 g m^{-2}, and liquid water content profiles can be derived with relative accuracies of ∼30%.

1.   Introduction

[2]   Precise quantification of the atmospheric state is essential for climate research and for weather prediction. The bulk of atmospheric profiling has historically been undertaken by routine radiosonde ascents, but worldwide the density of the radiosonde network is under pressure. Until this day no real alternatives to radiosonde soundings have been operationally established. Clearly, radiosonde soundings state benchmark measurements when it comes to profiling the atmosphere. However, carrying out radiosonde ascents on a routine basis presents enormous cost and labor factors. Typically operational radiosonde sites launch upper air soundings on a 12-hourly basis, so that short-lived weather events will not be captured. Also, single ascents need ∼1 hour to profile the troposphere and also underlie wind drifts effects. Another drawback concerning radiosonde ascents is that no methods have been established to measure liquid water on an operational basis. Generally in situ measurements of liquid water can only be obtained by employing costly aircraft measurements carrying suited instruments which, e.g., evaluate the light scattered by the droplets. Cost-effective and operational measurements of cloud liquid water content would be of high value for the evaluation and further development of numerical weather prediction (NWP) and climate models, where mostly only crude microphysical schemes are used to calculate the cloud and the successive precipitation development. One demanding question that still has not been resolved in this context is to what extent a ground-based remote sensing site could complement or even partially substitute parts of an operational radiosonde network.

[1]Meteorological Institute, University of Munich, Munich, Germany.
[2]Royal Netherlands Meteorological Institute, De Bilt, Netherlands.

[3] It has been known for some time that passive microwave radiometry offers the potential of filling the gap in retrieving the atmospheric thermodynamic state [*Westwater*, 1997], i.e., the distribution of temperature, humidity and liquid water, in a quasi-continuous and instantaneous way. This requires a retrieval model, which transforms the measured radiative quantities into thermodynamic information. In general, the retrieval problem is underdetermined, implying that no unique solution of the thermodynamic structure exists in correspondence to the measurements. Rather, a wide range of possible thermodynamic structures cause the same measured radiative quantities, so that further assumptions and additional measurements are needed to narrow down the range of valid thermodynamic solutions. Moreover, the vertical resolution of a typical microwave profiler in a stand-alone operation mode for temperature and humidity retrieval is very limited [e.g., *Güldner and Spänkuch*, 2001]. *Cadeddu et al.* [2002] have applied a multiresolution wavelet transform technique for studying the vertical resolution of temperature profiles from a multifrequency microwave profiler and found rapidly degrading values of 125 m in 400 m height to about 500 m in 1.5 km height at zenith viewing direction.

[4] To overcome the aforementioned deficiencies of a stand-alone instrument, this study makes use of sensor synergy from a number of atmospheric sensors. In the approach presented here, a continuous retrieval of the vertically resolved atmospheric parameters temperature, humidity and liquid water is achieved by employing a ground-based profiling station, where simultaneous and collocated measurements of a microwave profiler, a cloud radar and a lidar ceilometer are combined with a priori information obtained from the closest operational radiosonde sounding. The cloud radar and lidar ceilometer are capable of unambiguously locating a cloud in the vertical and thus fill a major gap left by microwave observations. How such measurements can be combined in an optimal way was shown by *Löhnert et al.* [2004] who introduced an integrated profiling technique (IPT) for the combination of the aforementioned measurements. The work by *Löhnert et al.* [2004], while comprehensive, can be expanded and refined considerably because it is expected that the inclusion of a succession of additional parameters in the IPT routine will further improve the technique of retrieving the atmospheric state.

[5] The purpose of this paper is to address the accuracy of the contemporary IPT. It is our goal to show how close remote sensing measurements can get to describing the actual atmospheric state, with specific focus on the temperature, humidity and liquid water structure. This research is timely because remote sensing technology is becoming more and more accurate and affordable and microwave profilers and cloud radars have been or are being set up at a number of remote sensing sites over Europe, the United States and other parts of the world (http://www.cloud-net.org, http://www.arm.gov).

[6] A general problem is that it is not possible to assess the accuracy of the retrieval method since the true state required to validate the retrieved state is unknown. This applies in particular to the cloudy component of the atmospheric state. For example, in situ liquid water measurements are only sparsely available from aircraft, which themselves exhibit large measurement uncertainties. However, even with aircraft it is impossible to probe the vertical column probed by a ground-based profiling station in an instantaneous manner. Therefore the accuracy assessment is performed within a state-of-the-art model environment, so that the atmospheric state and the measurements can be accessed at an arbitrary time and location. A further benefit of such an approach is that the impact of the a priori temperature and humidity profiles information supplied to the IPT can be very effectively evaluated as a function of time and space with respect to the actual measurement.

[7] The method of assessment is described in section 2, where section 2.1 depicts our general strategy, section 2.2 describes the atmospheric state and measurement vectors and also shows how the model measurements are converted to the atmospheric state via the so-called forward model. The inversion theory, i.e., the IPT retrieval scheme, is illustrated in section 2.3, while section 2.4 deals with a number of specific issues arising from the atmospheric model that we chose to represent the real world. In section 3 the IPT retrieval accuracy is discussed by comparing the retrieved states to the original states of the atmospheric model. The focus lies on evaluating retrievals of temperature and humidity profiles as a function of time and space from the a priori profile (sections 3.1 and 3.2), and on the liquid water vertical structure (section 3.3). Finally, in section 4, we summarize our results and assess the implications on climate monitoring and weather prediction.

2. Method of Accuracy Assessment

2.1. Strategy

[8] To overcome the problem inherent in validating the IPT technique with real world data we apply an atmospheric model in order to create an artificial true atmospheric state. This is the state we would like to recover by supplying the IPT with the remote sensing measurements (Figure 1). Within the model world, measurements in the usual sense of output from real instrumental devices do not exist. Instead, virtual instrumental devices or forward models are used to calculate simulated measurements from the given atmospheric state (i.e., temperature, pressure, humidity, cloud position, cloud microphysics). The great advantage of this process is that we can completely exclude systematic measurement errors as well as systematic errors due to uncertainties in radiative transfer, which are almost impossible to quantify in reality. On the other hand, in order to produce realistic retrieval results, noisy errors typical for each measurement have been included. Hence the results presented in the following sections highlight the theoretical potential of a physically based retrieval method for retrieving the true atmospheric state.

[9] A possible disadvantage of the approach using the atmospheric model as a "test bed" may be that the artificial atmospheric states may not cover the complete range of observable atmospheric states. A consequence might be that the accuracy assessment is restricted to the model world itself. In order to transfer the findings to the real world, the assumption must be made that the state-of-the-art atmospheric model represents the atmospheric state in a realistic manner, at least concerning the mean state and the variability. The validity of such assumptions can be tested by
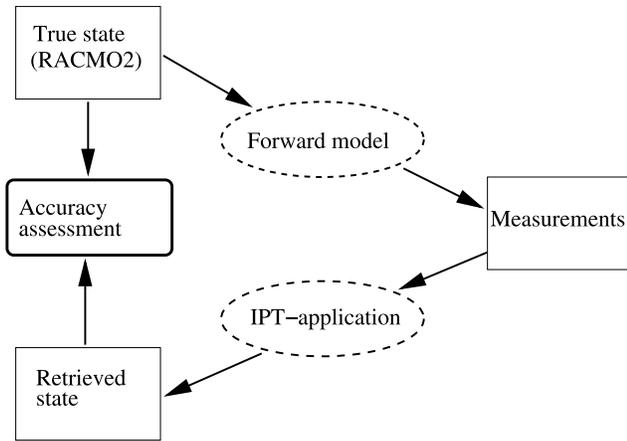
Figure 1. Schematic concept of the experimental setup applied in this study.

evaluating atmospheric models with measurements from long-term observational campaigns like the European cloudnet project or the U.S. Atmospheric Radiation Measurement (ARM).

2.2. State Vector, Measurement Vector, and Forward Model

[10] The atmospheric model supplies the true atmospheric state vector $\mathbf{x}$ to be retrieved, which consists of vertical profiles of atmospheric temperature ($\mathbf{T}$), absolute humidity ($\boldsymbol{\rho_v}$) and cloud liquid water content ($\mathbf{LWC}$), such that we can notate $\mathbf{x} = (\mathbf{T}, \boldsymbol{\rho_v}, \log_{10}(\mathbf{LWC}))$. From here on profile vectors will be noted in bold. We retrieve $\log_{10}(\mathbf{LWC})$ instead of directly $\mathbf{LWC}$, because the distribution of $\log_{10}(LWC)$ more closely resembles a Gaussian shape than LWC (see section 2.3) and additionally, we do not have to worry about negative LWC values within the retrieval procedure. Multiple liquid water cloud layers are also retrieved and state no limitation to the method. The vertical resolution is set to 250 m in the lowest 5 km and to 500 m from 5 to 10 km, where the atmosphere has been cut off synthetically. This leads to a total of 31 atmospherics levels, which we will denote with *nlevel* from here on. A forward model operator F is applied to $\mathbf{x}$ leading to the measurement vector $\mathbf{y}$, which consists of the parameters actually measurable by the instruments, namely brightness temperatures (TB) from the microwave profiler, radar reflectivities (Z) from the cloud radar, and the surface meteorological measurements of temperature and humidity (T_{gr} and $\rho_{v,gr}$). This means that the measurement vector takes the following form

$$\mathbf{y} = \begin{pmatrix} TB_1 \\ \dots \\ TB_{19} \\ Z_1 \\ \dots \\ Z_{ncld} \\ T_{gr} \\ \rho_{v,gr} \end{pmatrix}. \tag{1}$$

[11] The brightness temperatures ($TB_1 \dots TB_{19}$) are obtained from the given atmospheric state by applying the radiative transfer operator RTO:

$$TB_i = \mathrm{RTO}(\mathbf{T}, \boldsymbol{\rho_v}, \mathbf{p}, \mathbf{LWC}, f_i), \tag{2}$$

where the f_i denote the microwave frequencies. Here we utilize the 19 distinct frequencies of the 22-channel microwave profiler MICCY [*Crewell et al.*, 2001] with $f = (22.235, 22.985, 23.735, 24.485, 25.235, 25.985, 26.735, 27.485, 28.235, 50.800, 51.800, 52.800, 53.800, 54.800, 55.800, 56.800, 57.800, 58.800, 90.000$ GHz). The remaining three channels of MICCY are used to probe information on polarization, which we do not employ here. Since the profile of atmospheric pressure $\mathbf{p}$ is relevant for radiative transfer, but is not be retrieved, we take $\mathbf{p}$ as a given parameter. We assume that $\mathbf{p}$ at time of the measurement is equal to the closest available operational radiosonde profile of $\mathbf{p}$. The specified RTO performs the microwave radiative transfer only for nonscattering cases. This approximation is justified for nonprecipitating clouds and frequencies below ~100 GHz [*Simmer*, 1994]. Microwave absorption for water vapor and oxygen is calculated according to *Rosenkranz* [1998]. To speed up the calculations we have made use of the Fast Absorber Predictor (FAP) scheme for gaseous absorbers [*Löhnert et al.*, 2004], which basically, at a specified level, relates ambient temperature, humidity and pressure to the total microwave absorption via linear regression, whereby the bias-corrected FAP RMS accuracy is mostly on the same order as the RMS difference between the *Liebe et al.* [1993] and Rosenkranz absorption models and never exceeds ~0.7 K. The FAP scheme is on the order of $10\times$ faster than the original absorption codes. The time factor is critical for calculating the Jacobians (see section 2.3). Microwave absorption for liquid water is calculated according to *Liebe et al.* [1993].

[12] In the retrieval scheme the radar reflectivities are used as a physical constraint concerning the position of the cloud in the vertical. Additionally, Z itself contains a certain amount of information on LWC. The cloud radar reflectivities $Z_1 \dots Z_{ncld}$ in *ncld* detected cloud layers are calculated from the LWC profile (dimension: *ncld*) via a power law relation of the form

$$Z = b_1 \cdot LWC^{b_2}, \tag{3}$$

whereby a cloud layer denotes the space between two adjacent levels and a cloud is assumed to exist if the threshold of 10^{-6} kg kg^{-1} in LWC is exceeded within the 250 m layer. The coefficients b_1 and b_2 are derived from a singular column cloud microphysical model according to *Issig* [1997]. The microphysics of this model is spectrally resolved, meaning that cloud liquid water is calculated for 40 different radius bins. This allows the exact calculation of Z because the radar reflectivity is equal to the sixth moment of the droplet size spectrum. Accordingly b_1 and b_2 can be determined by performing a linear regression between $\log(Z)$ and $\log(LWC)$. Additionally, in this case, b_1 and b_2 were calculated as a function of height above cloud base

and cloud vertical extent (see *Löhnert et al.* [2001] for a detailed description). However, because of the above mentioned dependency to the sixth moment of droplet size distribution, this relation alone is far too inaccurate for reliable LWC results.

[13] The final components of the measurement vector, the near surface values of temperature T_{gr} and humidity $\rho_{v,gr}$ are directly taken from the lowest model level, which is located at $\sim$10 m above the surface.

[14] To make our experimental setup as realistic as possible, we have included random noise to the measurement vector. The *TB*s have been contaminated with Gaussian noise of 0.5 K, which should more than account for radiometric and calibration noise of state-of-the-art microwave profilers. The *Z* values have been contaminated with 1 dBZ noise and T_{gr} and $\rho_{v,gr}$ with 0.5 K and 0.1 g m^{-3}, respectively.

2.3. Inversion of the Measurement

[15] Section 2.1 describes the method of determining the measurement vector $\mathbf{y}$ from the state vector $\mathbf{x}$, which is straightforward. This section now describes the inversion procedure, i.e., how to determine $\mathbf{x}$ given $\mathbf{y}$. The IPT is applied to the measurement vector $\mathbf{y}$ with the goal of retrieving the atmospheric state vector $\mathbf{x}$ in an optimal way. The method is described in detail by *Löhnert et al.* [2004] and highlights the benefits of combining a microwave profiler with a cloud radar for simultaneously retrieving **T**, $\boldsymbol{\rho_v}$ and **LWC**. As mentioned above, determining $\mathbf{x}$ from $\mathbf{y}$ directly is an underdetermined and ill-conditioned problem, meaning that no unique solution exists and that very small errors in the measurement will lead to huge deviations in the atmospheric profile. A way to solve this problem is to combine the measurements with a priori information, i.e., information about the atmospheric state which is given prior to the measurement. The optimal estimation equations [e.g., *Rodgers*, 2000] are suited for combining such pieces of measurement and a priori information. An optimal atmospheric state $\mathbf{x}_{op}$ can be found by iterating the following formulation

$$\mathbf{x}_{i+1} = \mathbf{x}_i + \left(\mathbf{K}_i^T \mathbf{S}_e^{-1} \mathbf{K}_i + \mathbf{S}_a^{-1}\right)^{-1}$$
$$\times \left[\mathbf{K}_i^T \mathbf{S}_e^{-1}(\mathbf{y} - \mathbf{y}_i) + \mathbf{S}_a^{-1}(\mathbf{x}_a - \mathbf{x}_i)\right], \quad (4)$$

where i represents the iteration step, $\mathbf{x}_a$ the a priori profiles of T, ρ_v and LWC, $\mathbf{S}_a$ the a priori covariance matrix and $\mathbf{S}_e$ the combined measurement and forward model error covariance matrix. $\mathbf{K}_i = \partial \mathrm{F}(\mathbf{x}_i)/\partial \mathbf{x}_i = \partial \mathbf{y}_i/\partial \mathbf{x}_i$ represents the so-called Jacobian, or the sensitivity of the forward model to changes in $\mathbf{x}$, whereby $\mathbf{K}_i$ is recalculated for each iteration. Optimally, the formulation of equation (4) should guarantee the minimization of a quadratic cost function between $\mathbf{x}_a$ and $\mathbf{x}_i$, and $\mathbf{y}$ and $\mathbf{y}_i$, respectively, when the difference between $\mathbf{x}_{i+1}$ and $\mathbf{x}_i$ goes toward zero. The iteration procedure is terminated after an optimal number of iterations ($i = op$) when IPT has converged satisfactorily (for more on the convergence criterion refer to *Löhnert et al.* [2004]. It is important to note that the solution $\mathbf{x}_{op}$ must be interpreted as the most probable solution of a Gaussian

distributed probability density function, whose covariance can be written as

$$\mathbf{S}_{op} = \left(\mathbf{K}_{op}^T \mathbf{S}_e^{-1} \mathbf{K}_{op} + \mathbf{S}_a^{-1}\right)^{-1}. \quad (5)$$

[16] The diagonal elements of this matrix give an estimate of the mean quadratic error of $\mathbf{x}_{op}$, whereas the off-diagonal elements yield information on the correlation of retrieval errors between the different heights.

[17] As a further constraint to minimize the degrees of freedom, the humidity is set to its saturation value within the detected cloud boundaries. The saturation value of ρ_v in a specific cloud layer is determined using the corresponding T value of the prior iteration. For the first iteration, the first guess value of T is used.

[18] Typically, the a priori information will be compiled from a climatology or provided by a radiosonde ascent or even a model forecast. In the model world utilized in this paper, we assume to know the profiles from an operational radiosonde ascent, which was launched at distance Δd from the measurement site and valid at time Δt prior to the measurement. This was done in order to simulate the information that IPT usually extracts from radiosonde observations. In the accuracy assessment carried out Δt has been varied from 0 to 12 hours, in correspondence to the standard routine operation that radiosondes are normally launched every 12 hours, and Δd has been varied from 0 to $\sim$500 km. The sensitivity of the accuracy to the spatial and temporal distance of the a priori information to the measurement site will be addressed in section 3.2. In this study we have assumed two approaches to constructing the a priori information: the nowcasting (NC) and the climate (CL) modes.

[19] In the NC mode we assume to have access only to the latest radiosonde information before the time of the measurement; for example, at 1500 LT (local time) the a priori data would be taken from the 1200 LT sounding, assuming that, ideally, the soundings are launched at 0000 and 1200 LT. The NC attribute originates from the possible application of this kind of a priori data; it can be used to calculate thermodynamic profiles online with the IPT, once measurement and a priori data have been collected. To construct a representative a priori covariance matrix $\mathbf{S}_a$, the assumption of taking the 1200 (0000) LT sounding as a proxy for the actual temperature and humidity profiles between 1200 (0000) and 2400 (1200) LT has been validated on a statistical basis. This information has been derived by evaluating the atmospheric model output (N_{eval} evaluations) in the following way:

$$\mathbf{S}_{a,i,j} = \frac{\sum_{k=1}^{N_{eval}} \left(v_{a,i} - v_i\right)_k \cdot \left(v_{a,j} - v_j\right)_k}{N_{eval} - 1}, \quad (6)$$

where i,j range between 1 and 2*nlevel, a value i,j between 1 and *nlevel* indicating the variable temperature and a value of i,j between *nlevel*+1 and 2*nlevel the variable humidity. Then the diagonal entries of $\mathbf{S}_a$ are the mean square differences between the a priori variables (v_a) and the true variables (v) at each height ($i = j$). Correspondingly, the off-

diagonal entries (covariances) are calculated as the mean product of $v_a - v$ at one height and $v_a - v$ at another height ($i \neq j$). Note that the full covariance matrix is calculated, meaning that covariances are also calculated between temperature and humidity. Not all model output was used to calculate $\mathbf{S}_a$, but only model output at 3-hourly equidistant time steps. This means, e.g., that between the radiosonde launches at 0 and 12 UTC the variables v and v_a at 0300, 0600 and 0900 UTC are used to calculate $\mathbf{S}_a$ (correspondingly 1500, 1800 and 2100 UTC between the 1200 and 0000 UTC launches).

[20] In the application of the CL mode we assume that the measurements (remote and in situ) have been taken at some time in the past and we want to reconstruct the best possible thermodynamic state of the atmosphere, in the sense of a reanalysis. The a priori profiles of T and ρ_v are now calculated by linear temporal interpolation at each height between two consecutive radiosondes. The evaluation of these a priori profiles for T and ρ_v is performed according to equation (6) in the same manner as in the NC mode.

[21] The LWC components of the covariance matrix are calculated totally independently of the T and ρ_v components, implying that the a priori covariances between these parameters are inherently set to zero. As an a priori profile we assume an average LWC profile derived from many realizations of the cloud microphysical model (section 2.2). Again, as in case of the Z-LWC power law relations, this profile was calculated as a function of height above cloud base and cloud vertical extent. Correspondingly, for each cloud vertical extent, a LWC covariance matrix has been calculated, where the maximum cloud vertical extent had to be set to 1500 m. The reasons for this were that the microphysical model did not produce a sufficiently large number of nonprecipitating cases with vertical extents larger than 1500 m, so that a statistically significant covariance matrix could not be calculated for these cases (for details, see Löhnert et al. [2001]). This means that the IPT version presented here can only be applied to cases where liquid clouds do not exceed a vertical extent of 1500 m.

[22] In this study the $\mathbf{S}_e$ matrix is calculated as follows. For the first 19×19 components, which correspond to the MICCY measurements, a typical value for a squared TB error due to random calibration and radiometric noise is set to 0.25 K^2 for each frequency. It is assumed that these errors are independent; thus they only contribute to the diagonal components of $\mathbf{S}_e$. Further, the error covariances due to the FAP are considered in the first 19×19 components, which are calculated by considering the differences between the original absorption model and the FAP. Note that the covariances between each of the channels are considered in the off-diagonal components of $\mathbf{S}_e$. The following *ncld* diagonal components represent the squared errors of Z due to random radar calibration uncertainty (1 dBZ^2), but also errors due to the uncertainty of the Z-LWC relationship. The latter have also been derived by using output from the cloud microphysical model described in section 2.2 and are again a function of height above cloud base and cloud vertical extent. The components for T_{gr} and $\rho_{v,gr}$ are simply the square of the error values noted in section 2.2 and only contribute to the last two diagonal $\mathbf{S}_e$ components.

2.4. Specifics of Experimental Setup

[23] To generate a time series of "true" states by a large-scale atmospheric model, the following requirements must apply. It is important that the model carries LWC as an independent prognostic variable, and does not diagnose LWC as a function of relative humidity. The latter would imply too strong restrictions on the possible outcomes for T, ρ_v and LWC. Though the actual skill scores of the model are not of relevance for this study, a certain level of realism of the model is required, meaning that the model should produce temporal and spatial variations in the state variables with amplitudes and frequencies that are comparable to what is seen in observations. The model output has to be physically consistent and it should preferably include the lower stratosphere. Finally, the model should be able to produce a temporal record that is sufficiently long to cover a number of weather regime changes. It is also preferable that the record is genuinely uninterrupted, such as in a climate type run, in order to avoid discontinuities like in a series of weather forecasts.

[24] Any present-day climate model would typically meet these requirements. Here we have operated the Regional Atmospheric Climate Model (RACMO2) [Lenderink et al., 2003; de Bruijn and van Meijgaard, 2004] developed at the Royal Netherlands Meteorological Institute (KNMI). The model combines a recent version of the High-Resolution Limited Area Model (HIRLAM) NWP dynamical core (5.0.6) with a version of the parameterization package of physical processes used by the European Centre for Medium-Range Weather Forecast (ECMWF) model, i.e., cycle 23 release 4 (CY23R4). This release has also been used in the ECMWF reanalysis project ERA40 (http://www.ecmwf.int/research/era/). A detailed description of the physics package is found in work by White [2002], or available online at http://www.ecmwf.int/research/ifsdocs/. The model has been operated on a domain covering western Europe (126×130 grid points) at 18 km horizontal resolution and with 40 layers in the vertical. A climate type run has been performed for the 2-month period August–September 2001, starting on 1 August 2001, 0000 UTC. This period marks the first BBC campaign [Crewell et al., 2005]. This campaign was part of the European CLIWA-Net (Cloud Liquid Water Network) project, which involved the setup of a prototype of a European cloud observing network and the use of CLIWA-Net observations in model evaluation [van Meijgaard and Crewell, 2005]. Lateral forcings and sea surface temperatures are taken from ECMWF analyses. For an arbitrary model grid point direct model output of temperature, humidity and cloud parameters (i.e., liquid water content and cloud vertical extent) is stored at 15 min temporal resolution resulting in a uninterrupted time series of 5855 records per grid point. Here we have selected the model grid point nearest to Cabauw, Netherlands (4.93°E, 51.93°N) to serve as the receptor point, which is the location of the CESAR, the Cabauw Experimental Site for Atmospheric Research of KNMI. This major remote sensing site provides all the instruments (and many more) mentioned in this study.

[25] For inferring the TBs the RTO has been operated on the grid box mean model state variables rather than on pure cloudy states. This modus operandi implies that we need to adjust the humidity constraint to saturation within the cloud

boundaries (section 2.1). Like virtually all present-day climate models, RACMO2 utilizes a cloud scheme in order to represent subgrid-scale cloud processes within a model grid box in each model layer. The outcome of the cloud scheme essentially assumes that a grid cell can be divided into one cloudy part with fraction C_f and a cloud free part with fraction $(1-C_f)$. All liquid water mass is in the cloudy part, LWC_c, and conditions are at saturation, $\rho_{v,c} = \rho_{v,sat}$. There is no liquid water loading in the cloud free environment, $LWC_e = 0$, the humidity is subsaturated, $\rho_{v,e} < \rho_{v,sat}$. Temperature is not assumed to be subject to subgrid-scale effects. Grid box mean quantities are derived according to

$$m = C_f \cdot m_c + (1 - C_f) \cdot m_e, \tag{7}$$

where m is any quantity. Hence, for nonzero grid box mean liquid water contents it is no longer appropriate to assume that conditions are saturated, but we must allow them to be subsaturated. This can be achieved by relaxing the humidity constraint according to

$$\rho_v = RH \cdot \rho_{v,sat}(T,p), \tag{8}$$

where RH is the grid box mean relative humidity of the cloudy model layer.

[26] To adapt to the current limits of the IPT [see *Löhnert et al.*, 2004], contributions to TBs coming from liquid water clouds at altitudes above 5 km have been suppressed. Since the current IPT cannot be applied to precipitating cases, contributions from liquid precipitative fluxes have also been neglected. Additionally, because the ice phase is not retrieved, ice produced by the model has been neglected for the calculation of the TBs and Z.

[27] Owing to the fact that the model does not provide any information on the cloud particle size distribution (rather only on LWC), an accurate calculation of Z is impossible. Following *Liao and Sassen* [1994], the radar reflectivity Z of a model layer containing liquid water can be calculated according to the power law relation

$$Z = \frac{3.6}{N}(LWC)^{(1/0.56)}, \tag{9}$$

where N represents the cloud droplet number density in units cm^{-3} and LWC and Z are here expressed in units g cm^{-3} and mm^6 m^{-3}, respectively. Because RACMO2 does not employ the number density as a model parameter, it has to be predetermined to simulate the real world in which the number density can realistically vary between 50 and 300 per cm^3 depending on the aerosol loading. This leads to a parameterization of N as a function of the wind direction, since in the Cabauw region wind direction can be considered a reasonable proxy for the aerosol loading. When the wind has a northwesterly component relatively clean air with low aerosol loadings is imported from the North Sea, whereas the opposite applies when flow has a southeasterly component from the European continent. The wind direction is easily available in the RACMO2 model,

but is, however, not part of the measurement vector **y**. The precise relation we have used is

$$N = 0.5 \cdot (N_{\min} + N_{\max}) + 0.5 \cdot (N_{\min} - N_{\max}) \\ \cdot \cos\left(\frac{2\pi \cdot (d - \alpha_{\min})}{360}\right), \tag{10}$$

where $N_{\min}$ and $N_{\max}$ label the minimum and maximum values for the droplet numbers, 50 and 300 cm^{-3}, respectively, d denotes the model wind direction in the specified cloud layer in degrees, while $\alpha_{\min}$, set to 315°, indicates the wind direction where N reaches its minimum.

[28] It is now possible to calculate Z in a realistic manner from RACMO2 model output by employing equations (9) and (10) which we consider as the measurement "truth." The precise details of this parameterization are irrelevant; the only thing that matters is that noise is introduced in the relation between Z and LWC in a quasi-realistic manner. However, when solving the inverse problem, we use equation (3) to infer LWC from Z because we cannot measure N.

3. Evaluation and Results

[29] In the following the results of the temperature, humidity and LWC profiles are analyzed in detail. A common error measure is the systematic or bias error defined as

$$\text{BIAS} = \frac{\sum_{i=1}^{N} x_{i,ret} - x_{i,truth}}{N_{eval}}, \tag{11}$$

with N_{eval} denoting the number of evaluations, and $x_{i,ret}$ and $x_{i,truth}$ the retrieved and "true" model state, respectively. Also, we will use the so-called absolute bias, defined as

$$\text{AB} = \left|\frac{\sum_{i=1}^{N} x_{i,ret} - x_{i,truth}}{N_{eval}}\right|, \tag{12}$$

which is simply the absolute value of equation (11).

[30] Additionally, we use the root mean square (RMS) error to characterize the random error. Generally the RMS error is defined as

$$\text{RMS} = \sqrt{\frac{\sum_{i=1}^{N} \left(x_{i,ret} - x_{i,truth}\right)^2}{N_{eval} - 1}}; \tag{13}$$

however, in the following we will exclusively use a corrected formulation to ensure that systematic differences are without influence on the RMS value, leading to the following formulation:

$$\text{RMS}_{corrected} = \sqrt{\frac{\sum_{i=1}^{N} \left(x_{i,ret} - m \cdot x_{i,truth} + b\right)^2}{N_{eval} - 1}}, \tag{14}$$

with m and b denoting the slope, and the offset, respectively, of the linear regression between $x_{i,ret}$ and $x_{i,truth}$.

[31] In total, the RACMO2 data set consists of 5855 cases at the receptor Cabauw of which 85% are cloudy and 15% are clear sky. These numbers agree quite well with the degree of cloudiness observed during the BBC campaign [van Meijgaard and Crewell, 2005] when the amount of clear-sky conditions was found to range between 15 to 11% for time intervals of aggregation between 10 and 30 min.

3.1. Retrieval of Temperature and Humidity Profiles at the Radiosonde Site

[32] In this section the results for temperature and humidity profiles for the continuous NC and CL application modes are shown, assuming that the a priori measurements are taken at the same location as the measurements contained in the measurement vector $\mathbf{y}$. From the total number of 5855, the IPT could only be successfully applied to a subset of 2385 ($\sim$41%) cases. This is largely due to the restriction regarding the maximum cloud vertical extent of 1500 m (section 2.3). Consequently, IPT was not applied to the 3357 ($\sim$57%) of the RACMO2 cases, which exhibited liquid clouds with vertical extents larger than 1500 m. The remaining 113 ($\sim$2%) cases showed convergence problems and were excluded from the following analysis.

[33] For the NC mode accuracies presented in Figure 2, the a priori profile is assumed to consist of the latest radiosonde ascent, which is available at 0000 and 1200 LT. This means that for measurements taken between 0000 and 1200 LT, the 0000 LT ascent is used for $\mathbf{T}$ and $\rho_{\mathbf{v}}$ a priori information and for measurements between 1200 and 2400 LT, correspondingly the 1200 LT ascent is used. Because of this setup of the experiment, the time interval between measurement and a priori profile may vary between 0 and 12 hours. Next to the IPT RMS errors resulting from the IPT application, the RMS errors resulting from assuming the persistence of the a priori profile (a priori RMS) are also shown in Figures 2a and 2b. The difference between these two RMS errors can be called retrieval profit, indicating the benefit arising from the combination of all measurements compared to the radiosonde alone. For temperature (Figure 2a), as expected, we see the highest retrieval profit in the lowest 2 km, which is due to the fact that here the information content supplied by the microwave profiler is the highest. In the 0−2 km range the average profit is $\sim$0.7 K at an IPT RMS error of 0.7 K, whereas in the 0−4 km range the overall profit is 0.4 K at an IPT RMS error of 0.8 K. The gradual profit decrease with height can be explained by the exponential decay of the temperature weighting functions with height of the MICCY channels 50.8−58.8 GHz. Additionally shown in Figure 2a is the error derived from the $\mathbf{S}_{op}$ matrix (equation (5)), here referred to as the theoretical IPT error. If derived IPT RMS and theoretical IPT error match well, this may be seen as an indication that the retrieval system is working correctly. Throughout the profile, these two errors show a similar shape, with deviations seldom larger than 0.2 K. The fact the IPT RMS error is slightly larger than the theoretical IPT error in the lowest 4 km can be explained by the fact that the $\mathbf{S}_a$ matrix was not derived using the full data between the 0000 and 1200 UTC radiosondes but only 3-hourly samples (section 2.2). Thus a certain amount of variability is

missing in the $\mathbf{S}_{op}$ calculation. The corresponding RMS plot for humidity (Figure 2b) shows a maximum retrieval profit at approximately 1.2 km of $\sim$0.7 g m^{-3}. In the 0−2 km range the average profit is $\sim$0.5 g m^{-3} at an IPT RMS error of 0.7 g m^{-3}, whereas in the 0−6 km range the overall profit is 0.4 g m^{-3} at an IPT RMS error of 0.5 g m^{-3}. Compared to the temperature profile evaluation, the retrieval profit due to the additional remote sensing and surface-based measurements is found more pronounced for humidity and is also found to extend to higher altitudes, with significant profits up to $\sim$6 km height. This is due to the fact that here the water vapor information content included in the 22.235−28.235 GHz channels is relatively constant with height. The decay of the IPT accuracy beginning at $\sim$2 km is then due to the exponential decrease of absolute humidity with height. IPT RMS error and the predicted theoretical error show similar behavior as in the temperature case. Again, the slightly lower values of the theoretical error are attributed to the way $\mathbf{S}_{op}$ is calculated.

[34] Because of the fact that the IPT could only be successfully applied to a subset of the RACMO2 model output, the a priori bias errors of temperature and humidity are not zero, as would be expected from purely Gaussian distributed a priori information (Figures 2c and 2d). If the whole RACMO2 output set is regarded, the average a priori bias errors in both cases are very close to zero. The fact that systematic errors may arise in case of application to specific cases is of course a general problem, which will also arise during algorithm application in the "real world." However, the profiles of temperature and humidity IPT bias error are close to zero, with maximum absolute values of 0.2 K and 0.2 g m^{-3}, respectively. This shows that the IPT procedure can, to a certain extent, correct for systematic errors contained in the a priori data.

[35] Also shown in Figure 2 are the results one obtains using a "purely" statistical algorithm, explained below. Naturally, advantages of such statistical algorithms are that they are much easier to develop and to apply. In this case, multilinear regressions between brightness temperatures and physical temperature, respectively absolute humidity have been performed. The MICCY channels between 50.8 and 58.8 GHz were chosen for the temperature retrieval and the channels between 22.235 and 28.235 GHz were taken for the humidity retrieval. The regressions are based on a 10 year data set of the Dutch radiosonde station De Bilt, in this case only using the months August and September. Figures 2a and 2b make clear that the IPT outperforms the statistical retrieval throughout the profile in terms of RMS and bias error. The smaller RMS errors both for temperature and humidity make clear that a physically constrained algorithm, such as the IPT, together with sensible a priori profiles can give rise to higher accuracies than commonly used statistical algorithms. The bias error characteristics make especially clear that purely statistical algorithms are very much dependent on the climatology used for training. Bias errors in the range of 1 K and 0.5 g m^{-3} in the lowest 4 km of the atmosphere as shown here are not uncommon for such types of retrievals. Again, the significantly different statistical properties of the IPT applicable subset compared to the 10 year August/September climatology are a reason for these large systematic errors. On average, the IPT will never produce such a high bias error because of the fact that
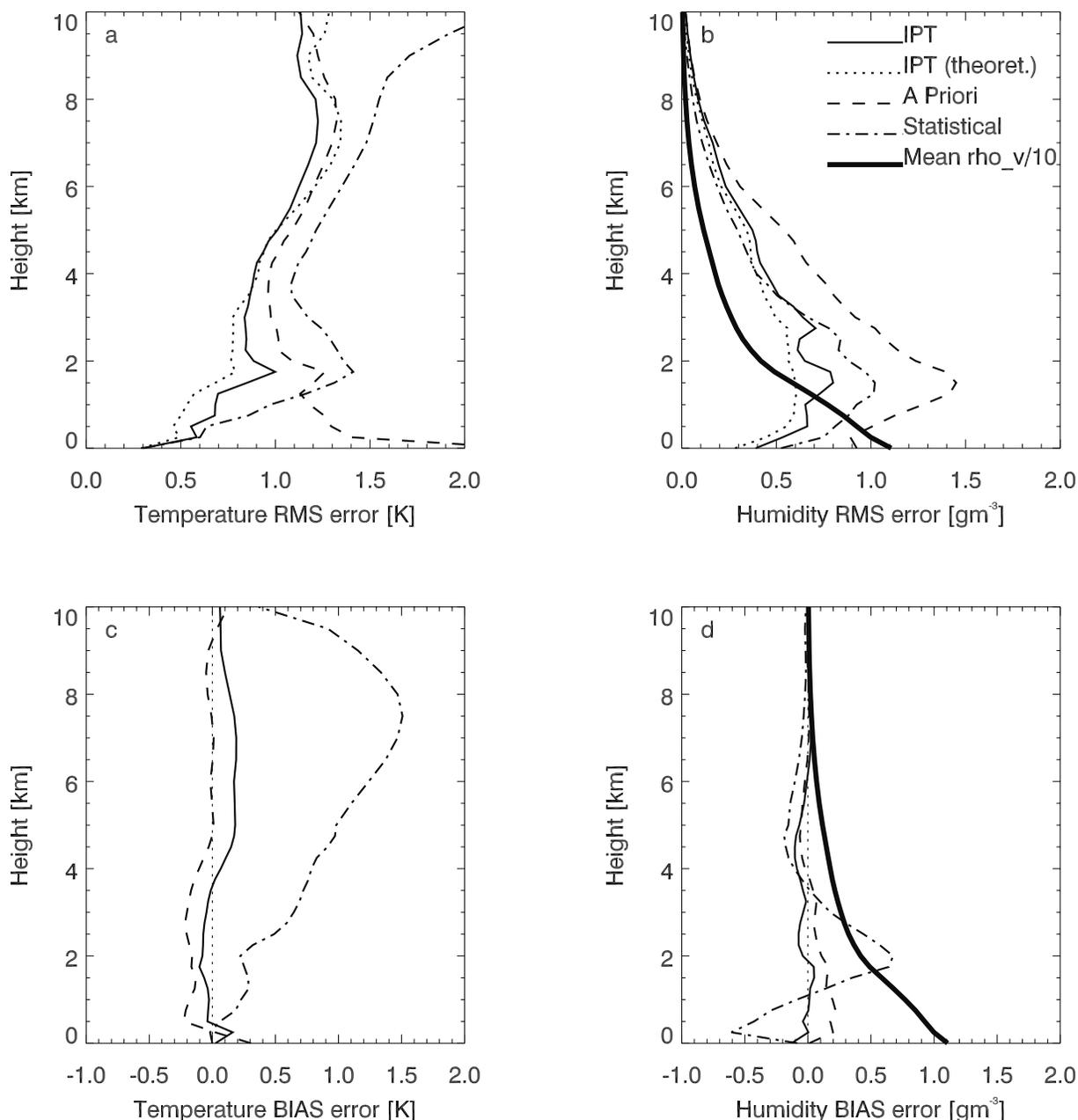
Figure 2. Accuracies of (a, c) temperature and (b, d) absolute humidity profiles for the nowcasting (NC) application mode. RMS errors are shown in Figures 1a and 1b, and bias errors are shown in Figures 1c and 1d. Shown are IPT accuracies (thin solid line), theoretical IPT accuracies (RMS only, dotted line), a priori accuracies (dashed line), and statistical retrieval accuracies (dash-dotted line). Subtracting the dashed lines from the bold lines in the RMS plots can be interpreted as the retrieval profit due to the IPT procedure. For orientation, the thick solid line in Figures 1b and 1d shows the mean profile of absolute humidity divided by 10.

the a priori data always consists of closely situated information from a radiosonde ascent.

[36] The accuracies of an IPT-like method in case of rapidly changing weather events are of special interest in data assimilation or nowcasting studies. In order to demonstrate IPT performance during rapidly changing weather events, the RACMO2 data set has been analyzed for events, where within 6 hours, the integrated water vapor changed by more than 5 kg m^{-2} or the temperature at 1500 m changed by more than 3 K. For these cases, in the 0−2 km range the average RMS error is 0.8 K, in the 0−4 km 0.9 K. In case of absolute humidity, the corresponding values are 0.7 g m^{-3} and 0.8 g m^{-3}, respectively. These numbers are only slightly poorer than those considering all the cases and show that the IPT is also capable of retrieving accurate temperature and humidity profiles in highly variable weather conditions.
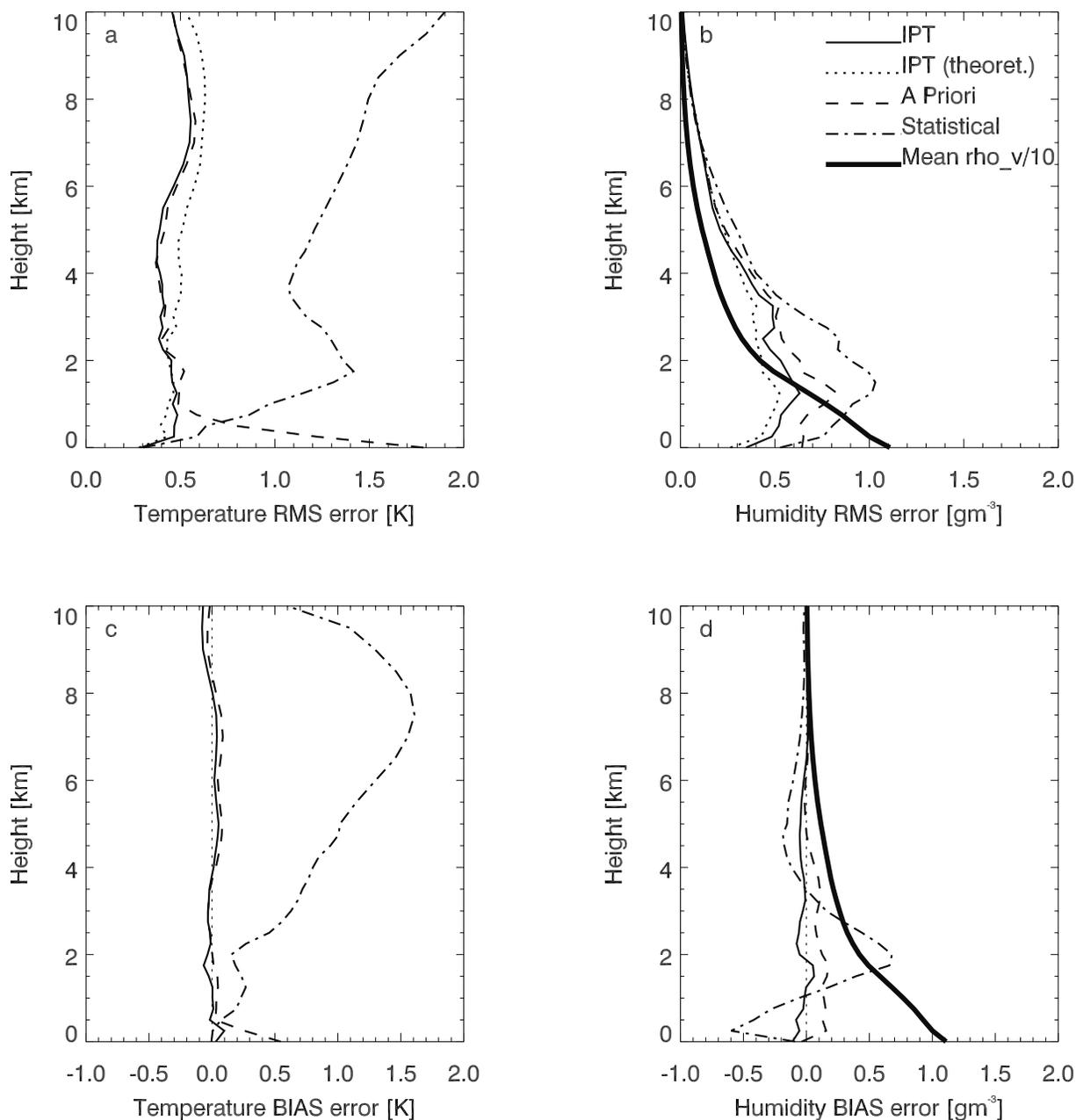
Figure 3. Same as Figure 2 but for climate (CL) application mode.

[37] In contrast to the application in NC mode, Figure 3 shows the results for the application in climate mode CL. As stated in section 2.3, the T and ρ_v a priori profiles are now a linear interpolation in time, either between the 0000 LT and 1200 LT or the 1200 LT and 2400 LT radiosonde ascents, depending on the time of measurement. Again, we assume the continuous measurements to take place at the same location as the radiosonde ascent. Comparing to the NC application mode, the overall retrieval profit is now smaller, both for T and for ρ_v. A significant temperature profit can now only be identified at maximum up to 2 km (Figure 3a), with an average value of 0.3 K and an average IPT RMS error of 0.4 K. The slightly larger ($\sim$0.1 K) RMS errors of the theoretical IPT accuracy in comparison to the a priori RMS accuracy above 3 km results from the fact that the IPT

could not be applied to the whole model output set (from which S_a was calculated), but rather only to the subset mentioned above. This apparent inconsistency in RMS error difference can now be understood by noting that the whole model output set, which determines the theoretical IPT error, contains more variability than the subset. A significant humidity profit can be identified up to 3 km, whereby the average humidity profit is now 0.2 g m^{-3} at an average IPT RMS error of 0.5 g m^{-3} in the lowest 4 km (Figure 3b). This reduction in retrieval profit in comparison to the NC case is due to the fact that the CL a priori assumption is much more accurate than the NC assumption. However, the CL application can of course only be carried out, if, relative to the measurement time, the latest radiosonde ascent and the one in the nearest future are available

simultaneously. Using the CL approach, temperature and humidity IPT absolute bias (AB) error values are at maximum in the range of 0.1 K and 0.1 g m^{-3}, respectively (Figures 3c and 3d) with a priori AB errors slightly larger.

3.2. Retrieval of Temperature and Humidity Profiles Away From the Radiosonde Site

[38] Up to now all calculations have been carried out assuming that the a priori data and measurement data originate from the same location. In the following we carry out a sensitivity study, where the central question is: How accurate is the IPT if the a priori information comes from locations Δd km away from the point of measurement and also from discrete time periods Δt hours before the actual measurement? In this realization (in contrast to the setup in section 3.1) the temporal distance between measurement and a priori information is fixed to Δt. In case Δt were equal to 6 hours, the sample size of IPT applicable cases would be much too low because up to now we have assumed 0000 and 1200 UTC as the a priori (= radiosonde sounding) times and thus IPT application would only be possible at 0600 and 1800 UTC of each day. In order to obtain an equally large number of applicable cases as in section 3.1, it is assumed that the a priori profile is known for each time of measurement; that is, the profile at Δt hours before the measurement is assumed to be known. This is not a realistic approach, but it will artificially increase the sample size to create statistically significant results.

[39] Specifically, we evaluated cases for Δd = [0 km, 85 km, 510 km] and Δt = [0 hours, 6 hours, 12 hours], which results in nine possible $\Delta d/\Delta t$ combinations. However, the combination 0 h/0 km is not considered because here the a priori information is equal to the model truth and the additional measurements can by definition not contribute to any profit. For each of the remaining eight combinations, a separate a priori covariance matrix $\mathbf{S}_a$ was calculated. Principally $\mathbf{S}_a$ was calculated as denoted in equation (6) only that now v_a varies in time by precisely Δt, but also in space according to Δd. With this experiment setup we have generated eight IPT output applications, in which we can investigate the influence of the a priori profile as a function of Δd and Δt on the IPT retrieval accuracy. As in section 3.1 the eight IPT applications could also be successfully calculated for ∼40% of the total RACMO2 output set. We have chosen the spatial scale in order to evaluate the results on a common basis. This means that the Δt have been converted to the kilometer scale by using Taylor's hypothesis and a typical atmospheric propagation velocity of 10 m s^{-1}. The resulting distances were sorted into classes corresponding to the closest whole number dividable by 100. Combining the classes coming from Δd = [0 km, 85 km, 510 km] and Δt = [0 hours, 6 hours, 12 hours] results in seven spatial-scale classes (100, 200, 300, 400, 500, 700, 900 km) as shown in Figures 4 and 5. For example, the 900 km value represents the [Δd = 510 km, Δt = 12 hours] combination because 510 is rounded to 500 and 12 hours corresponds to 432 km, which is rounded to 400 km. For comparison note that in section 3.1, the a priori profiles were taken at Δd = 0 km, but Δt was encompassing *all* values from 0 to 12 hours, corresponding to 0−432 km.

[40] In order to obtain a better overview the following results are expressed in error measures that represent an average over the lowest 4 km. We have chosen 4 km because of the fact that the retrieval profit of the microwave profiler is only marginal above this height. As expected, Figure 4 shows increasing values of the 4 km−average a priori temperature RMS (calculated by applying equation (14) to the model truth and the a priori variable) with increasing kilometer scale. This is due to the fact that the a priori assumption gets worse with increasing spatial scale. In the first four spatial-scale classes, increasing values of average a priori temperature RMS are correlated with an increase of the average IPT RMS error rising from ∼0.5 to ∼1.0 K. For larger distances the average IPT RMS error is rather constant at values around 1.0−1.1 K. Approximately the same average IPT RMS error is obtained, if, instead of the radiosonde a priori information, the average temperature profile and the corresponding covariance matrix of a 10-year radiosonde data set (August/September) of the Dutch sounding station De Bilt are used as a priori information. Note that this approach does not correspond to the statistical retrieval in section 3.1, but rather states a solver for equation (4) using the modified a priori statistics. Figure 4 makes clear that for an a priori radiosonde ascent for spatial-scale distances larger than 300 km, the average IPT RMS temperature accuracy will not become better than in the case when a sensible climatological mean is used. This is interesting to note, because the average a priori RMS in the climatological cases has by far the largest RMS value. In this case, assuming the covariances between the levels are captured correctly, the microwave profiler information can lead to an average profit of more than 3 K in the lowest 4 km (Figure 4). However, if average IPT RMS accuracies of less than 1 K are to be achieved, the microwave profiler should be situated within a spatial-scale radius of say 200−300 km of the radiosonde measurement. Within this range, the retrieval profit by using the instrument combination is generally lower (because of the higher accuracy of the a priori information), however the accuracies are best. Similar evaluations have been carried out for the retrievals of absolute humidity (Figure 5). Here increasing values of the 4 km−average a priori RMS error can also be observed for spatial-scale distances up to 400 km, where saturation toward ∼1.3 g m^{-3} seems to take place. This saturation coincides with approximately constant average IPT RMS values of absolute humidity of 0.7−0.8 g m^{-3}. Accuracies of better than 0.5 g m^{-3} can only be obtained within a spatial-scale radius of 100 km of the radiosonde ascent. Again, if a climatological profile is used as a priori humidity information, the accuracies are in the same range as in the case when the radiosonde information corresponding to spatial-scale distances of 400 km and larger is used.

[41] Concerning the systematic errors, Figures 4 and 5 also show, for both temperature and humidity, the average AB errors. The average of the AB error is calculated by again averaging the AB error values over the lowest 4 km. Here, when taking the 4 km average, the AB error is used instead of the bias error to avoid that the bias errors over the 4 km height range will cancel out to zero. In this respect, the average AB error gives a measure for an overall systematic error. As can be seen in Figures 4 and 5, the 4 km−average a priori AB errors are quite significant starting at ∼400 km spatial scale. If, as noted in section 3.1, the whole RACMO2 output set is regarded, the average a priori AB
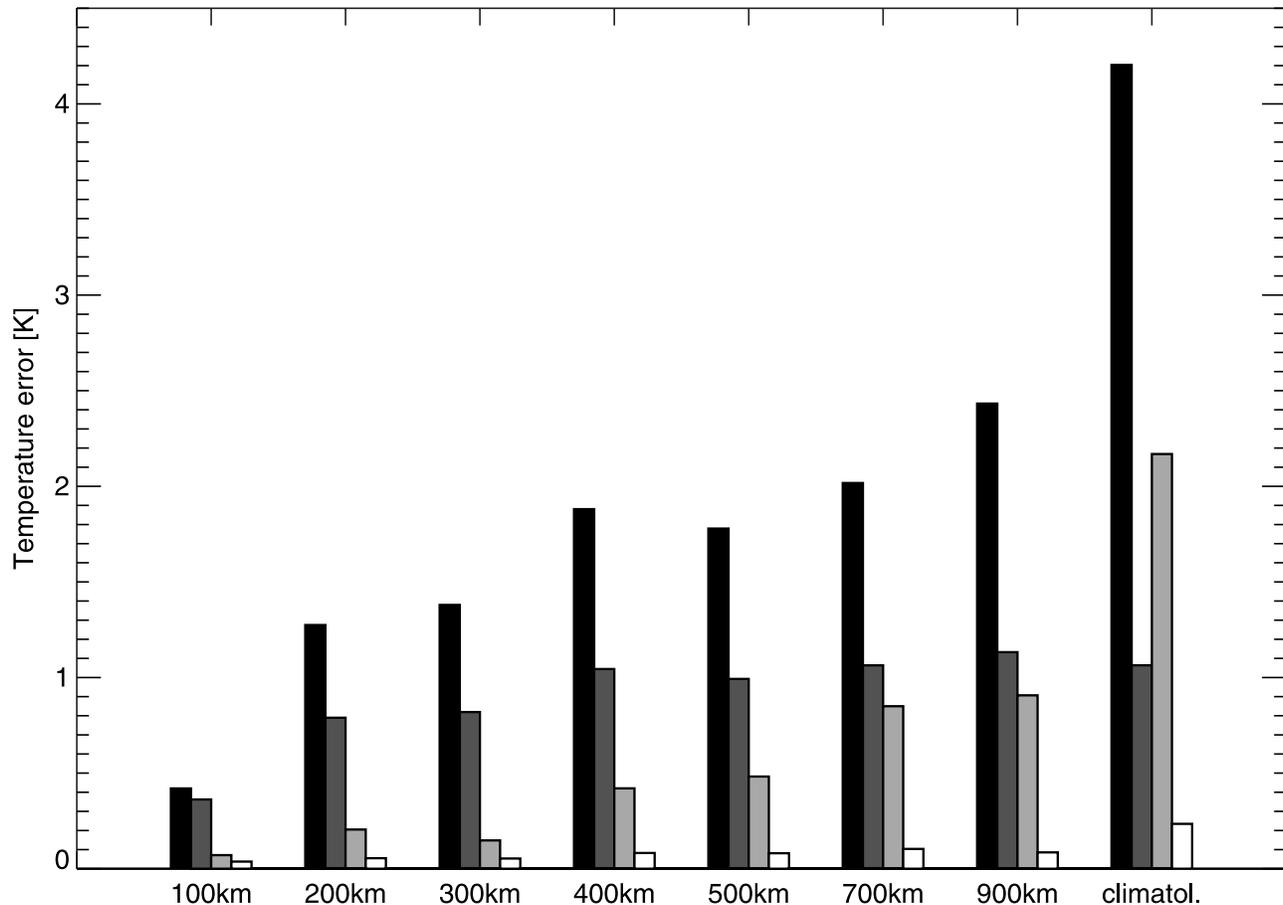
Figure 4. Average IPT and a priori accuracies for the lowest 4 km of the atmosphere as a function of the spatial scale to the radiosonde launch. Black bars show average RMS a priori errors in the lowest 4 km (assuming the persistent validity of the closest and latest radiosonde ascent). Dark gray bars show average of the RMS IPT errors in the lowest 4 km. Light gray bars show average of the absolute bias (AB) a priori errors in the lowest 4 km (assuming the persistent validity of the closest and latest radiosonde ascent). White bars show average of the AB IPT errors in the lowest 4 km. The last four bars (climatology) show results for the a priori data consisting of a T climatology.

errors are much closer to zero. This is again the result of relating the IPT application to a certain subset of the model output. This subset is not equally distributed over the August/September period and can thus show systematic deviations. However, it is encouraging to see that the average IPT AB errors are in turn lower than 0.1 K and 0.15 g m^{-3} for temperature, respectively absolute humidity. This means that the IPT procedure can essentially reduce systematic errors contained in the a priori data.

[42] This seems not to be the case if the IPT runs employing the 10-year a priori climatology are investigated. In case of temperature, if the whole RACMO2 model output set is regarded, the average a priori AB errors are no longer negligible and we thus see a relatively high a priori AB error of 2.2 K. Even in this AB error dominated case, the IPT application can reduce the average IPT AB error to below 0.3 K. If the a priori bias errors are subtracted from each profile before IPT application, the average IPT AB error is also close to 0 K, which gives confidence that the IPT performs in the desired linear manner. In the humidity case (Figure 5), the integrated water vapor (IWV) bias error as

deduced by IPT (not shown) is very close to zero, however the information content of the brightness temperatures in conjunction with the weak a priori estimate is not able to reduce the average IPT AB error.

3.3. Thermodynamic Profile Retrieval Within Liquid Clouds

[43] IPT evaluation for the LWC profiles has been carried out with respect to cloud vertical extent (Figure 6). For LWC evaluation, only the NC mode application at the same location of the radiosonde site has been chosen, since no significant differences in LWC retrieval are observed as a function of the T and ρ_v a priori profiles. The LWC a priori profiles chosen are also independent of location, and NC or CL mode application. In all cases the LWC a priori profile is taken from the statistics provided by the singular column microphysical model (section 2.2). As stated in section 2.3, currently only clouds with vertical extents of up to 1500 m can be handled within the IPT. Like for **T** and ρ_v, the vertical resolution of **LWC** is 250 m, which results in six classes of cloud vertical extent, in which in each case LWC
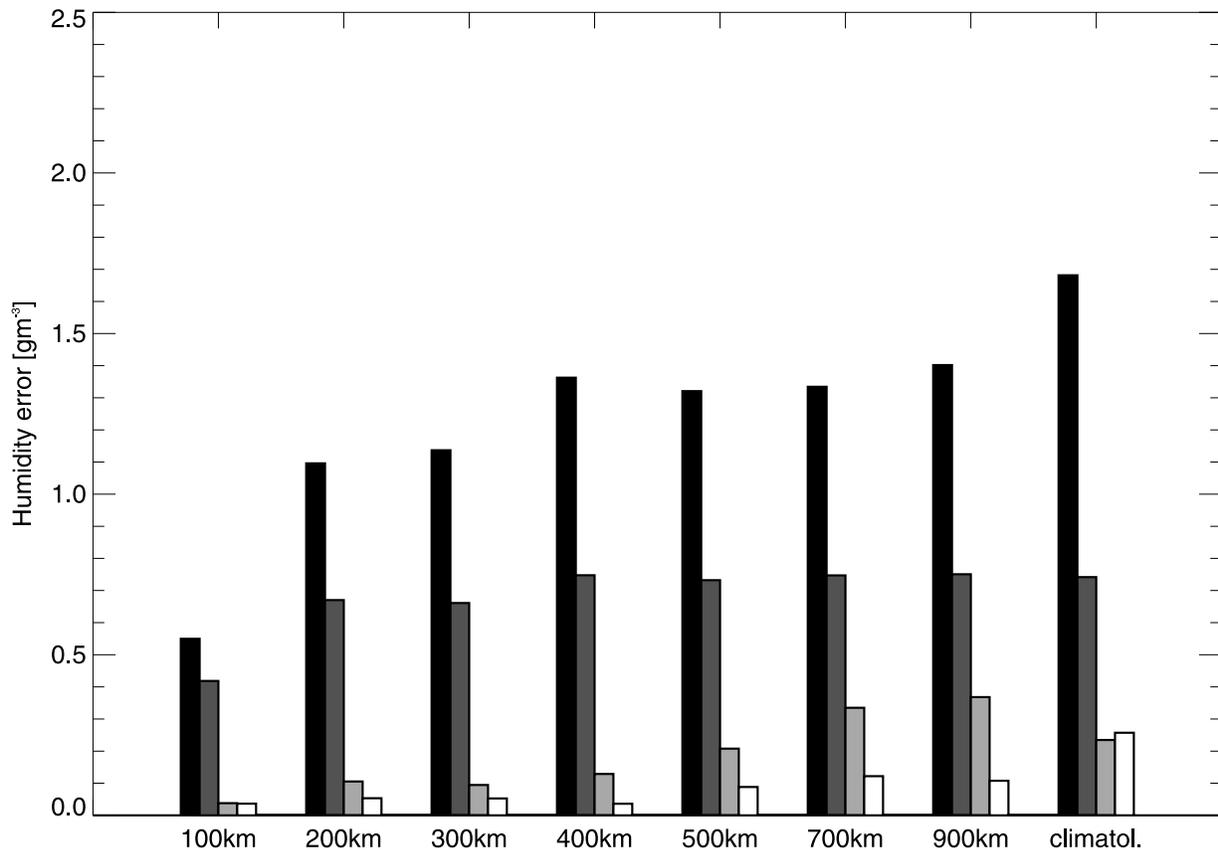
Figure 5. Same as Figure 4 but for absolute humidity.

is evaluated as a function of height above cloud base. Generally the LWC RMS errors increase with increasing cloud vertical extent; this is due to larger amounts of LWC in geometrically thicker clouds. As evident in Figure 6, the largest LWC RMS errors are correlated to the maximum LWC values within the profile. All in all, LWC RMS errors never exceed 25 mg m^{-3} (Figures 6a–6f). If the cloud layers closest to cloud top and cloud base are excluded from the analysis, the mean relative LWC error for clouds with vertical extents from 750 to 1500 m is approximately 30%. Also, the predicted theoretical IPT LWC errors are in rather good agreement with the derived RMS LWC errors. An exception is formed by the upper layers of the clouds with vertical extents of 1250 and 1500 m where the differences between these two parameters are in the order of 5 mg m^{-3}. Also shown in Figure 6 are the error curves corresponding to a standard LWC retrieval approach, where the Z-LWC relation is linearly scaled to match the liquid water path (LWP) measured by the microwave radiometer [e.g., *Frisch et al.*, 1998]. For cloud vertical extents larger than 500 m, the mean in-cloud improvement of the IPT with respect to the linear scaling method is ~10 mg m^{-3}, corresponding to a relative improvement of ~17%. The LWC bias characteristics (not shown) are negligible, if, again only the levels excluding the cloud boundaries are investigated. In this case, if all six cloud classes and all levels are analyzed, a mean in-cloud IPT LWC bias of +1 mg m^{-3} remains.

[44] Here we want to emphasize that application of the IPT results in a very improved performance concerning the retrieval of the integral quantities LWP and IWV. For LWP, the overall RMS error is 6 g m^{-2}, with a bias of +3 g m^{-2},

whereas for IWV the RMS error reaches 0.3 kg m^{-2}, with a bias error of −0.1 kg m^{-2}. These numbers are a factor 2–5 better than obtained with statistical methods using standard two-channel microwave radiometers [*Löhnert and Crewell*, 2003].

[45] One of the major benefits of microwave remote sensing is not only the retrieval of cloud properties, but also the possibility to retrieve temperature and humidity within clouds. This fact is demonstrated in Figures 7 and 8, where results for the NC application mode are shown. Again, as in the LWC evaluation, the results are classified in cloud thickness and are shown against "height above cloud base." In terms of temperature, the overall in-cloud retrieval profit is 0.5 K at an IPT RMS error of 0.7 K, which shows that the accuracy of the temperature retrieval within the cloud is on the same order as in the general clear and cloudy case (section 3.1). However, there is an overall positive IPT bias error of +0.2 K (Figure 7) in the IPT temperature retrieval, which is also present in the same magnitude in the a priori bias. Apparently, because of lack of constraints, the IPT is not capable of correcting for this a priori bias. Generally the a priori bias error is more pronounced, the thinner the cloud. A possible reason for this might be the more adiabatic character of thin, developing clouds. However, finding a plausible explanation for this behavior is complicated by the fact that this study is dealing with grid box mean model clouds instead of real clouds. In case of absolute humidity, the mean in-cloud IPT RMS error is 0.5 g m^{-3} and the retrieval profit is in the order of 0.7 g m^{-3}, which is a very satisfactory value and is even better than the values shown in Figure 2a for typical
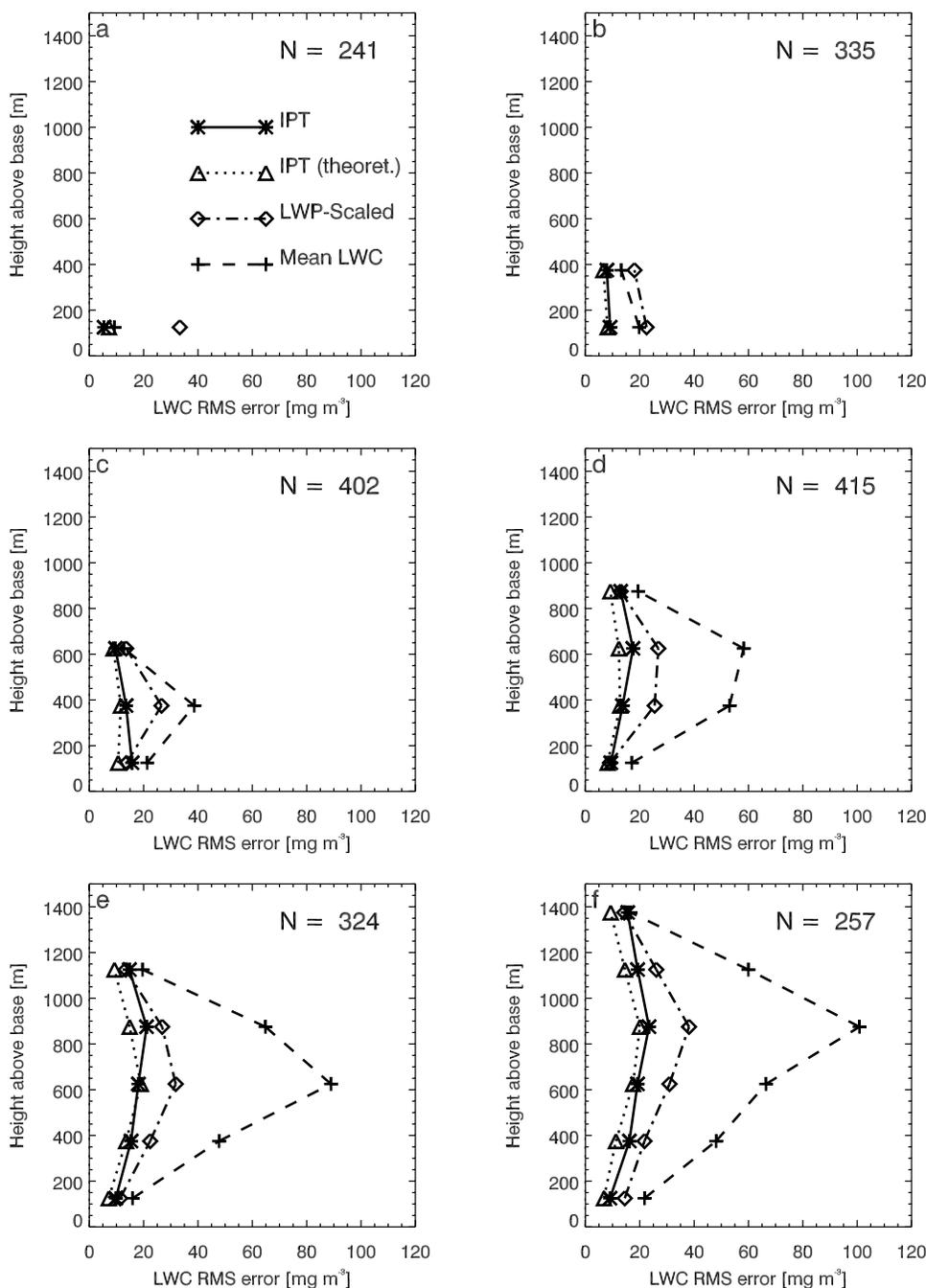
Figure 6. LWC RMS profile accuracies as a function of height above cloud base. The clouds are sorted into six classes of cloud vertical extent: (a) 250, (b) 500, (c) 750, (d) 1000, (e) 1250, and (f) 1500 m. The numbers in the top right corners indicate the total number of cloud realizations per cloud class. Shown are IPT accuracy (solid line with asterisks), theoretical IPT accuracy (dotted line with triangles), Z profile scaled linearly to microwave-derived LWP accuracy (dash-dotted line with diamonds), and average LWC values as comparison (dashed line with crosses).

cloud heights around 1 km. This improvement is due to the additional humidity constraint introduced by equation (8). The in-cloud a priori humidity error is slightly negative for almost all cloud levels and classes (overall value -0.13 g m^{-3}). This can be explained by the fact that the a priori humidity profile was derived for clear and cloudy atmospheres. This means that the average absolute humidity will be lower for the general case in comparison to the clouds-only case, since cloudy cases are correlated with

higher humidity values. However, by employing the above mentioned humidity constraint within the IPT application, this negative bias can be compensated to an overall value of ~ 0 g m^{-3}.

4. Discussion and Outlook

[46] Within this paper, we have tried to show how ground-based microwave remote sensors can be exploited
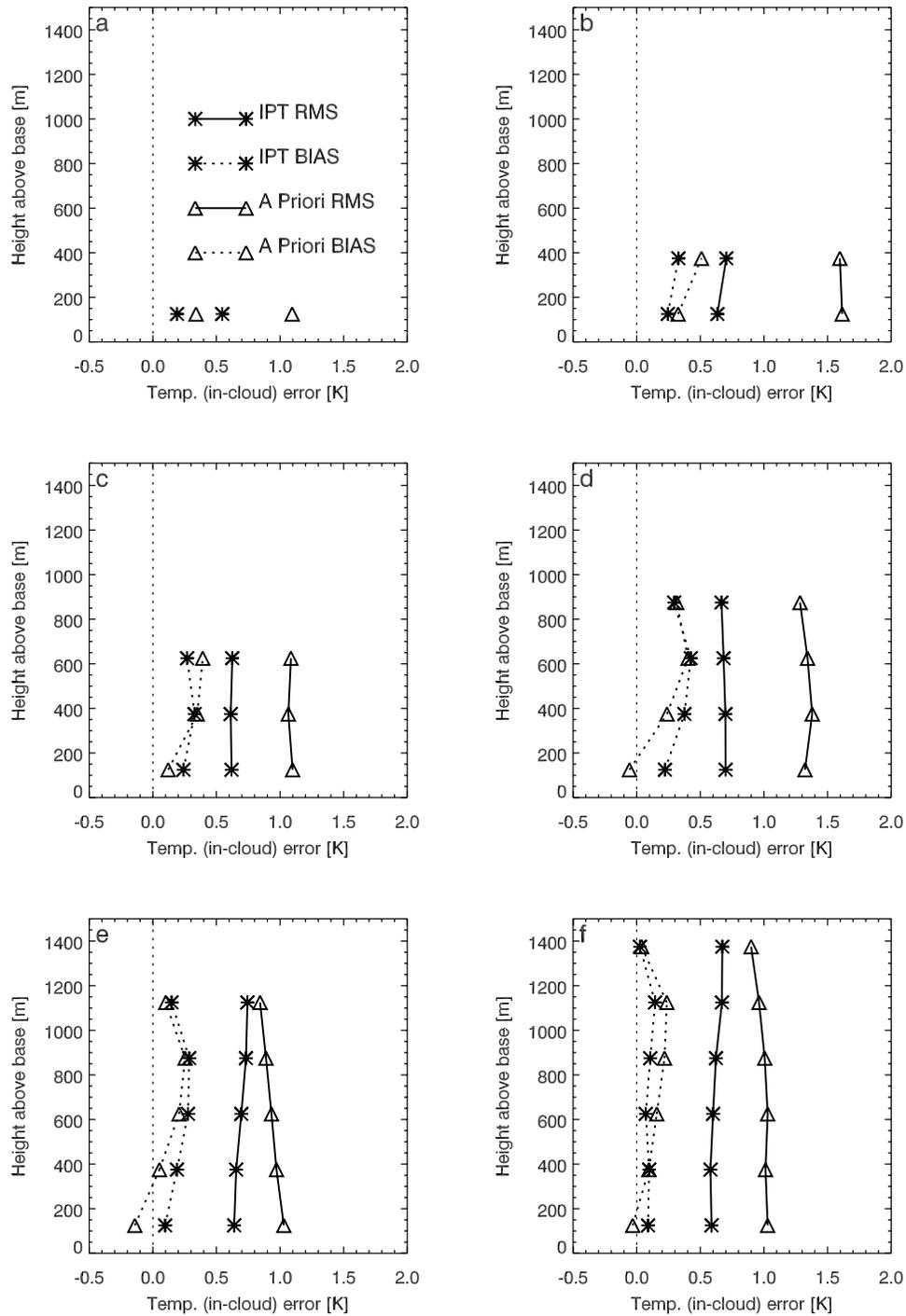
Figure 7. In-cloud temperature profile accuracies as a function of height above cloud base. The plots are sorted into the same six classes of cloud vertical extent as in Figure 6. IPT RMS error (bold line with asterisks), IPT bias (dotted line with asterisks), a priori RMS error (bold line with triangles), and a priori bias error (dotted line with triangles).

in an optimal sense with regard to the continuous retrieval of the thermodynamic state of the atmosphere. For the profile retrieval of temperature and humidity, the highest information content originates from the brightness temperature measurements of a microwave profiler such as MICCY. It is clear that such a microwave profiler—mainly because of restrictions in effective vertical resolution—

cannot reach the absolute accuracy of a radiosonde ascent, either in terms of temperature or humidity. However, we have demonstrated that microwave profilers can add a significant retrieval profit to the profiles in the time between two radiosonde ascents, either at the same location of the ascent or at different locations of up to 900 km away from the ascent.
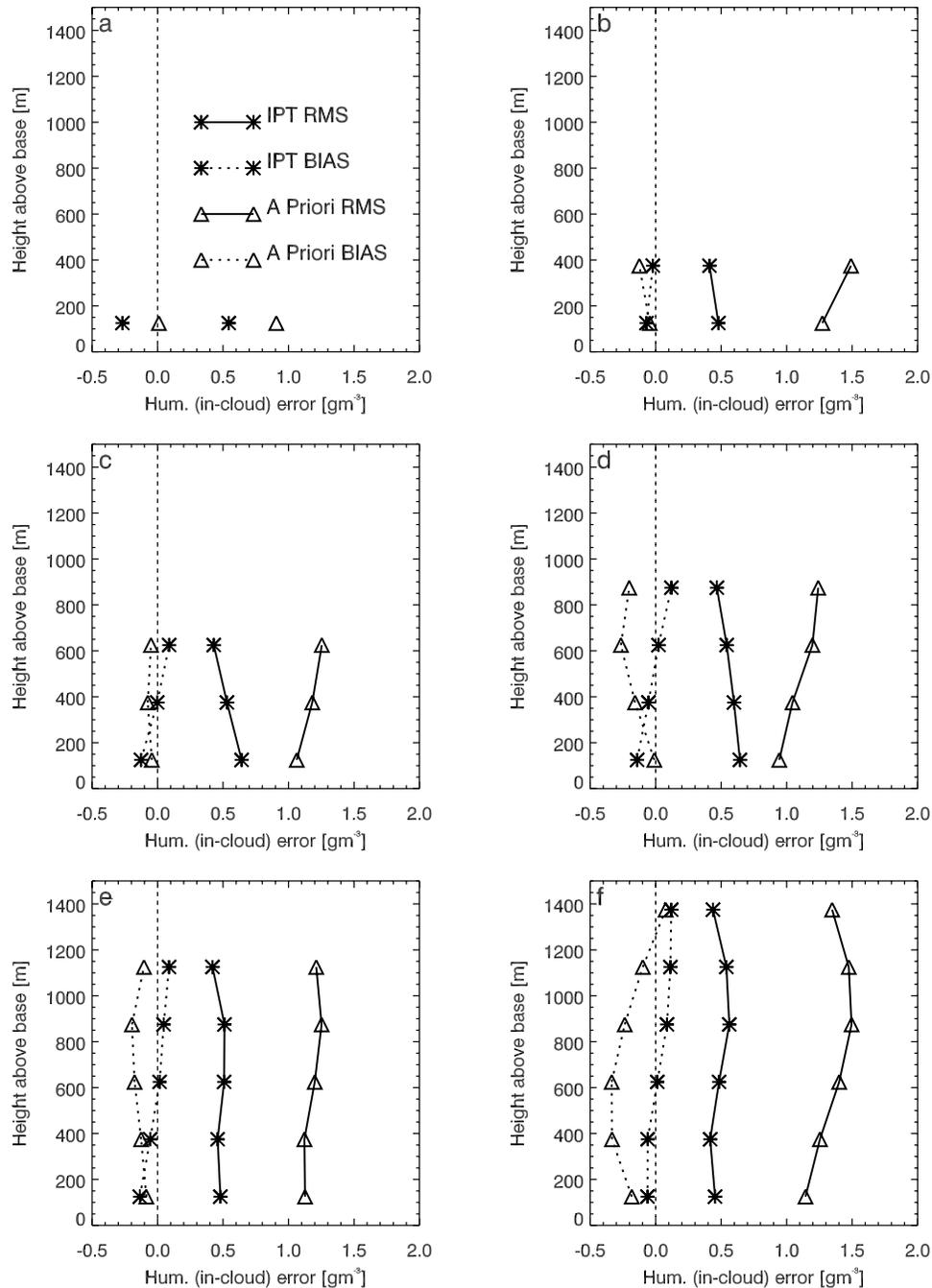
Figure 8. Same as Figure 7 but for in-cloud profiles of absolute humidity.

[47] Temperature and humidity profile retrievals have shown to be very dependent on the NC and CL application modes, whereas the LWC profile retrieval is less dependent on the mode of application. This is because in the presented experimental setup, the LWC a priori profile does not change in time and the covariances between temperature/ humidity and LWC are rather low. Generally, we expect that the NC application mode will be of major focus in future, because here the possibility exists for instantaneously retrieving the atmospheric thermodynamic state and thus this mode is suited for applications in nowcasting and data assimilation. The CL application mode is suited for the

reprocessing of data time series, e.g., for dedicated measurement campaigns, where it is of extreme importance to produce very accurate physically consistent profiles of the atmosphere using as many measurements and as much a priori information as possible.

[48] For the cloudy cases that could be analyzed, the IPT could reproduce the model LWC with mean accuracies of 30%. These LWC retrievals lead to overall LWP retrieval accuracies of below 10 g m^{-2}. This aspect is extremely important for the detection and retrieval of low-liquid water clouds, which have impact on the radiative budget. Analyzing the LWC profile retrieval, it was shown that the

IPT can outperform simple LWC retrieval methods, which scale the measured radar reflectivity profile to the microwave-derived LWP. Currently, the authors are working to improve the applied a priori LWC profile information. Future methods will provide a LWC a priori profile as a function of cloud vertical extent, cloud base temperature and statistical information about the nonadiabacity (dilution) of typical fair weather clouds. Such information will be obtained in the long-term sense by using cloudnet and US-ARM data sets. From such data sets it is expected to obtain the necessary cloud a priori information to describe clouds with vertical extents thicker than 1500 m.

[49] In the NC application case we have shown that one can continuously retrieve temperature and humidity profiles within the lowest 4 km of the atmosphere with average RMS accuracies of less than 1.1 K and 0.7 g m^{-3}, respectively. This is valid if the a priori information taken for the IPT consists merely of a sensible climatological mean of the station of measurement. However, caution must be taken considering the representativeness of the a priori information. For certain time periods, bias errors may be as large as the RMS errors. Significant improvements to this combined statistical/physical method can be obtained if the a priori information is taken from the closest operational radiosonde ascent. If the closest radiosonde ascent is within a spatial-temporal radius of 100 km (in our assumption 100 km would be equal to a temporal distance of ~3 hours), the average RMS accuracies for temperature profiles and humidity profiles within the lowest 4 km can be improved to values of 0.4 K, respectively 0.4 g m^{-3}, whereby the bias errors will be very close to 0 in both cases. Increasing this spatial-temporal distance will increase the retrieval profit with respect to the radiosonde; however, the RMS accuracies will gradually decrease.

[50] From the results we showed in section 3, an operational user has now the possibility of identifying the theoretical benefit (profit) associated to a profiling station with the IPT application. We have shown the RMS accuracies for the parameters temperature, humidity and LWC and also depict the profit one can derive from such a profiling system in contrast to regarding the a priori profile as the given truth. Principally, the user can now decide if a profiling station applying IPT is worth installing at a certain location or not. Four major benefits may arise from the installation of such a profiling station.

[51] 1. In comparison to radiosondes, the IPT can additionally retrieve multiple cloud base, cloud top and profiles of LWC, which can be very valuable for the initialization and evaluation of various atmospheric models. Additionally, valuable cloud climatologies may be derived.

[52] 2. Deployed at a radiosonde site, a profiling station employing an IPT can retrieve continuous profiles of temperature and humidity and capture atmospheric variability (e.g., diurnal cycle, frontal passage) which often cannot be measured by operationally launching radiosondes every 12 hours.

[53] 3. Deployed at a certain distance from an operational radiosonde site, the profiling station may complement an existing radiosonde network by adding extra temporal and spatial information. This may be especially valid in inhomogeneous terrain, where generally high spatial variability in temperature and humidity exists.

[54] 4. If the radiosonde network is very dense, one may consider replacing an operational radiosonde site with a profiling station applying IPT. Depending on the desired accuracies, the spatial-scale distances to the closest operational radiosonde should however not exceed 100–200 km. However, such a criterion would be up to the users and the accuracy they require.

[55] It may be interesting to note that central Europe (here including Austria, Belgium, Denmark, Germany, the Netherlands and Switzerland) has a relatively dense operational radiosonde network of in total 25 stations (http://www.metoffice.com/research/interproj/radiosonde/index.html) covering an area of 597 375 km^2, which implies that each radiosonde is representative for a radius of influence of ~87.2 km. The radiosonde networks of France or the United States (conterminous area), however, only possess radii of influence corresponding to ~157 km and ~196 km, respectively. In the dense European network and with the advent of ground-profiling stations, it may be worthwhile considering the replacement of a small number manpower- and cost-intensive radiosonde stations by a profiling station in future. However, this would of course only be promising, if additionally, a wind profiler would be incorporated into the profiling station, which has the capability of deriving the wind profile throughout the troposphere. In the less dense networks, additional profiling stations will provide an improvement toward continuously describing the atmospheric thermodynamic state in space and time.

[56] In the NC approach we have demonstrated the potential of the IPT using remote sensing measurements together with a priori data consisting of radiosonde ascents. Another approach however, might consist of using short-range forecast data itself as the a priori information, which may contain more information in comparison to the radiosonde data. However, in this case, the representativeness error [Kitchen, 1989] might need to be accounted for. This error accounts for the fact that a model grid box value (describing a domain mean) is used as a priori information for the retrieval at the remote sensing site, which states a spot measurement.

[57] Although the above presented results are encouraging, it must be mentioned that possible bias errors due to the radiative transfer operator and the instrument calibration have not been considered in this study. The main reasons for the systematic uncertainty of the radiative transfer operator can be found in description of microwave absorption due to gaseous components (oxygen and water vapor) and liquid water. Here, especially in the atmospheric windows, standard absorption models show systematic differences on the Kelvin scale [Melsheimer et al., 2005]. Also, receiver drifts and absolute calibration inaccuracies may also lead to longer-term instrumental offsets causing systematic offsets, typically also in the Kelvin range. Here, state-of-the-art microwave profilers (such as the RPG HATPRO generation [Rose et al., 2005]) can guarantee relatively high-accuracy and stable measurements. One major advantage of the here developed IPT-RACMO2 test bed is that such systematic errors can also be investigated in future. Systematic errors as a result of the instrument characteristics (these need to be known in detail) and varying absorption and their influence on the IPT-derived parameters may now be investigated in detail. This will help to see if instrument accuracy and

forward model accuracy are really suited in getting the results close to the theoretical possible ones highlighted in this study.

References

Cadeddu, M. P., G. E. Peckham, and C. Gaffard (2002), The vertical resolution of ground-based microwave radiometers analyzed through a multiresolution wavelet technique, *IEEE Trans. Geosci. Remote Sens.*, *40*, 531–540.

Crewell, S., H. Czekala, U. Löhnert, T. Rose, C. Simmer, R. Zimmermann, and R. Zimmermann (2001), Microwave radiometer for cloud cartography: A 22-channel ground-based microwave radiometer for atmospheric research, *Radio Sci.*, *36*, 621–638.

Crewell, S., et al. (2005), The BALTEX Bridge Campaign: An integrated approach for a better understanding of clouds, *Bull. Am. Meteorol. Soc.*, *85*(10), 1565–1584, doi:10.1175/BAMS-85-10-1565.

de Bruijn, E. I. F., and E. van Meijgaard (2004), Verification of HIRLAM with ECMWF physics compared with HIRLAM reference versions, *HIRLAM Tech. Rep.*, *63*, 39 pp., R. Neth. Meteorol. Inst., De Bilt, Netherlands. (Available at http://www.knmi.nl/publications/showBib. php?id=881.)

Frisch, A. S., C. W. Fairall, G. Feingold, T. Utal, and J. B. Snider (1998), On cloud radar and microwave radiometer measurements of stratus cloud liquid water profiles, *J. Geophys. Res.*, *103*, 23,195–23,197.

Güldner, J., and D. Spänkuch (2001), Remote sensing of the thermodynamic state of the atmospheric boundary layer by ground-based microwave radiometry, *J. Atmos. Oceanic Technol.*, *18*, 925–933.

Issig, C. (1997), Ein spektrales Wolkenmodell mit integriertem Strahlungsübertragungsmodell zur Unterstützung von Niederschlagsalgorithmen, Ph.D. dissertation, 119 pp., Univ. Bonn, Bonn, Germany.

Kitchen, M. (1989), Representativeness errors for radiosonde observations, *Q. J. R. Meteorol. Soc.*, *115*, 673–700.

Lenderink, G., B. van den Hurk, E. van Meijgaard, A. P. van Ulden, and J. H. Cuijpers (2003), Simulation of present-day climate in RACMO2: First results and model developments, *KNMI Tech. Rep. 252*, 24 pp., R. Neth. Meteorol. Inst., De Bilt, Netherlands.

Liao, L., and K. Sassen (1994), Investigation of relationships between Ka-band radar reflectivity and ice and liquid water contents, *Atmos. Res.*, *34*, 231–248.

Liebe, H. J., G. A. Hufford, and M. G. Cotton (1993), Propagation modelling of moist air and suspended water/ice particles at frequencies below 1000 GHz, *AGARD Conf. Proc.*, *P-542*, 3.1–3.10.

Löhnert, U., and S. Crewell (2003), Accuracy of cloud liquid water path from ground-based microwave radiometry: 1. Dependency on cloud model statistics, *Radio Sci.*, *38*(3), 8041, doi:10.1029/2002RS002654.

Löhnert, U., S. Crewell, A. Macke, and C. Simmer (2001), Profiling cloud liquid water by combining active and passive microwave measurements with cloud model statistics, *J. Atmos. Oceanic Technol.*, *18*, 1354–1366.

Löhnert, U., S. Crewell, and C. Simmer (2004), An integrated approach towards retrieving physically consistent profiles of temperature, humidity, and cloud liquid water, *J. Appl. Meteorol.*, *43*(9), 1295–1307.

Melsheimer, C., et al. (2005), Intercomparison of general purpose clear sky atmospheric radiative transfer models for the millimeter/submillimeter spectral range, *Radio Sci.*, *40*, RS1007, doi:10.1029/2004RS003110.

Rodgers, C. D. (2000), *Inverse Methods for Atmospheric Sounding: Theory and Practice*, 238 pp., World Sci., Hackensack, N. J.

Rose, T., S. Crewell, U. Löhnert, and C. Simmer (2005), A network suitable microwave radiometer for operational monitoring of the cloudy atmosphere, *Atmos. Res.*, *75*(3), 183–200, doi:10.1016/j.atmosres.2004.12.005.

Rosenkranz, P. W. (1998), Water vapor microwave continuum absorption: A comparison of measurements and models, *Radio Sci.*, *33*, 919–928.

Simmer, C. (1994), *Satellitenfernerkundung Hydrologischer Parameter der Atmosphäre mit Mikrowellen*, 313 pp., Verlag Dr. Kovac, Hamburg, Germany.

van Meijgaard, E., and S. Crewell (2005), Comparison of model predicted liquid water path with ground-based measurements during CLIWA-NET, *Atmos. Res.*, *75*(3), 201–226, doi:10.1016/j.atmosres.2004.12.006.

Westwater, E. R. (1997), Remote sensing of tropospheric temperature and water vapor by integrated observing systems, *Bull. Am. Meteorol. Soc.*, *78*, 1991–2006.

White, P. W., , (Ed.) (2002), Part IV, Physical processes (CY23R4), technical report, 101 pp., Eur. Cent. for Medium-Range Weather Forecasts, Reading, U. K. (Available at http://www.ecmwf.int/research/ifsdocs)

H. K. Baltink, R. Boers, and E. van Meijgaard, Royal Netherlands Meteorological Institute, NL-De Bilt 3730 AE, Netherlands.

S. Groß and U. Löhnert, Meteorological Institute, University of Munich, Theresienstraße 37, D-80333 Munich, Germany. (ulrich.loehnert@meteo.physik.uni-muenchen.de)